

Electronic Supplementary Information

Phase transition in WSe_{2-x}Te_x monolayers driven by charge injection and pressure: A first-principles study

Liyuan Chen,^a Li Chen,^a Hongli Chen,^a Kai Jiang,^a Liangqing Zhu,^a Liyan Shang,^a Yawei Li,^a Shijing Gong^a and Zhigao Hu^{*a,b}

^a Technical Center for Multifunctional Magneto-Optical Spectroscopy (Shanghai), Engineering Research Center of Nanophotonics & Advanced Instrument (Ministry of Education), Department of Physics, School of Physics and Electronic Science, East China Normal University, Shanghai 200241, China

^b Collaborative Innovation Center of Extreme Optics, Shanxi University, Taiyuan, Shanxi 030006, China

*Correspondence: (Z.G. Hu) zghu@ee.ecnu.edu.cn.

List of Contents:

Supplementary Note 1

Geometric structures of H and T' phases of WSe_{2-x}Te_x monolayers

Supplementary Note 2

AIMD simulations at room temperature for H and T' phases of WSe_{2-x}Te_x monolayers

Supplementary Note 3

AIMD simulations heated to 1100 K for WSe_{2-x}Te_x monolayers with high Te compositions

Supplementary Note 4

Band structures of H and T' phases of WSe_{2-x}Te_x monolayers

Supplementary Note 5

Charge injection and tensile strain regulate the phase transitions for MoSe_{2-x}Te_x and WSe_{2-x}S_x monolayers

Supplementary Note 1

Geometric structures of H and T' phases of $\text{WSe}_{2-x}\text{Te}_x$ monolayers:

We consider different configurations for H or T' phases of $\text{WSe}_{2-x}\text{Te}_x$ monolayers at the same Te concentration, and perform structural relaxation and electron self-consistency calculations. The most stable structures of H phase and T' phase at different concentrations are determined, as shown in Fig. S1. In addition, for the case of $x=1$, the minimum energy difference between different structural configurations in H phase is only 0.0005 eV/f.u., which indicates the coexistence of different configurations at the same concentration.

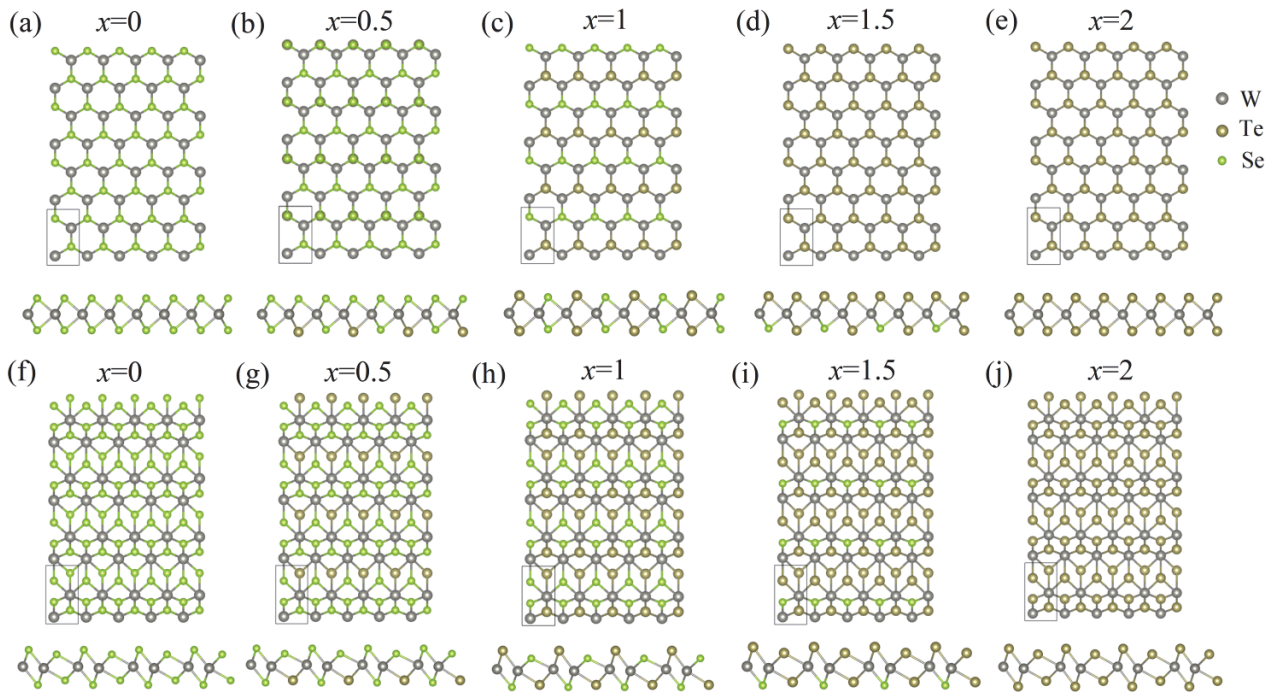


Fig. S1. Top and side view of (a-e) H phase and (f-j) T' phase of $\text{WSe}_{2-x}\text{Te}_x$ monolayers with different Te concentration.

Supplementary Note 2

AIMD simulations at room temperature for H and T' phases of WSe_{2-x}Te_x monolayers:

To further investigate the thermal stability of the two phases, the *ab initio* molecular dynamics (AIMD) simulations of the WSe_{2-x}Te_x monolayers are performed at 300 K, as shown in Fig. S2. A 120-atom supercell is used for AIMD simulations with one Γ point to sample the Brillouin zone integration. All the AIMD simulations were performed in the *NPT* ensemble (constant particle, pressure, and temperature) with 10000 step calculations at a time step of 3 fs. The free energy fluctuation curves show that the WSe_{2-x}Te_x monolayers hold stability at room temperature coherently, where the stable phase of WTe₂ is T' phase, whereas that of WSe₂ prefers the H phase. Comparing the initial structures with the equilibrium structures at 300 K, it can be seen that all the phase structures are not distorted or deformed because the average positions of the atoms are not drastically deviated.

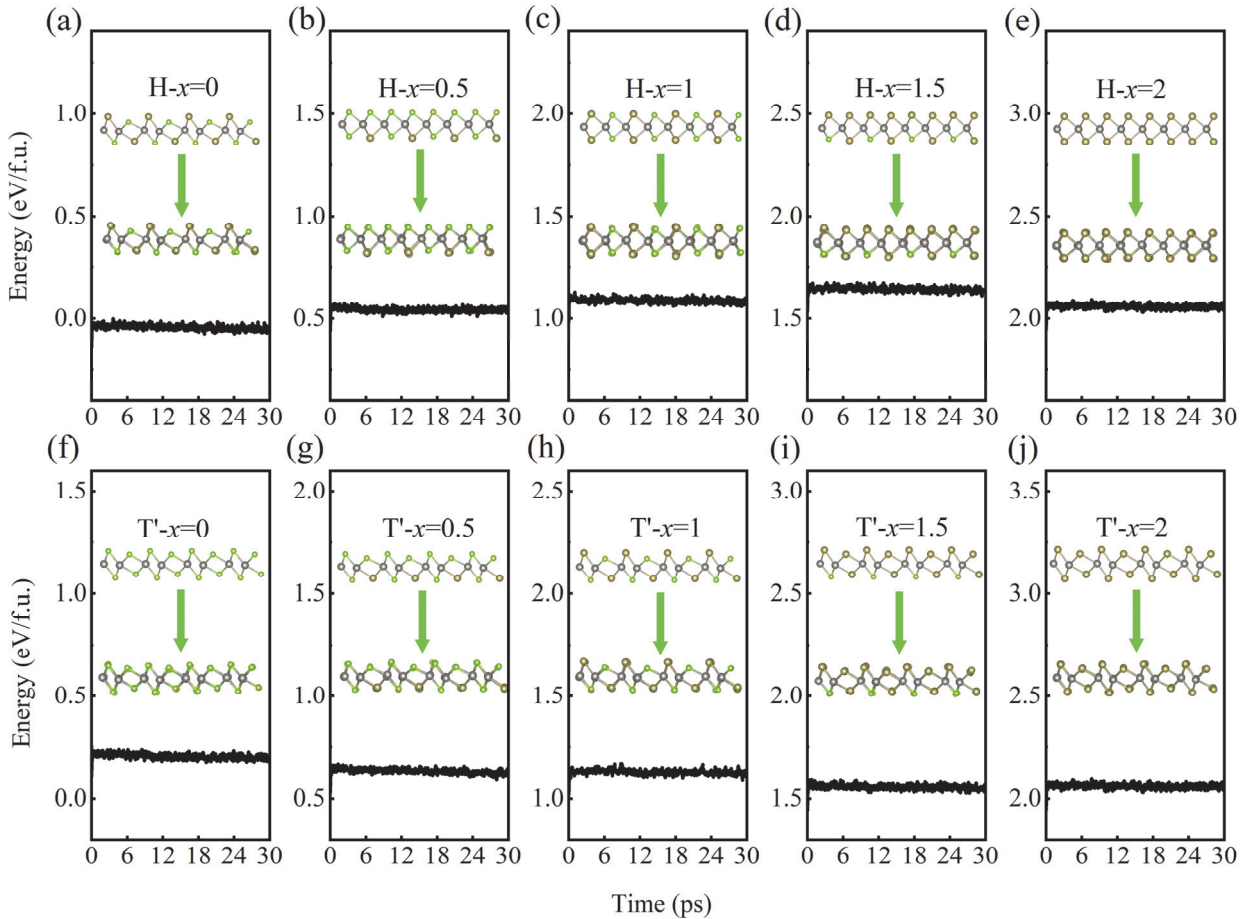


Fig. S2 Energy curves of AIMD simulations for (a-e) H-WSe_{2-x}Te_x and (f-j) T'-WSe_{2-x}Te_x at 300 K. The H-WSe_{2-x}Te_x at $x=0$ is used as the energy standard, and the ordinate unit is set to eV/f.u.. The illustrations show the initial structures and the equilibrium structures at 300 K.

Supplementary Note 3

AIMD simulations heated to 1100 K for WSe_{2-x}Te_x monolayers with high Te compositions:

After the atomic position relaxation and geometry optimization conducted in a static DFT calculation, a 120-atom supercell is used for AIMD simulations with one Γ point to sample the Brillouin zone integration. In order to dynamically monitor the phase transition of H-WSe_{2-x}Te_x monolayers with high Te composition, the H-WSe_{2-x}Te_x monolayer with $x=0$ was selected for comparison. The initial AIMD simulation was carried out, and the H-WSe_{2-x}Te_x monolayers with $x=0$, $x=1.5$ and $x=2$ were heated from 300 K to 1100 K, using 20000 step calculation with a time step of 1 fs. The temperature change curves of H-WSe_{2-x}Te_x monolayers at $x=0$, $x=1.5$ and $x=2$ tend to be consistent, as shown in Fig. S3a. In the process of heating and high-temperature hot bath, the adjacent W-W bonds in the H-WSe_{2-x}Te_x monolayers at $x=1.5$ and $x=2$ begin to evolve into long and short bonds, while the W-W bond length oscillates at the equilibrium position when $x=0$, as shown in Fig. S3c, d. In addition, the continuous hot bath at 1100 K changes the potential energy surfaces (PESs) for WSe_{2-x}Te_x monolayers of high Te concentration, providing the ability to manipulate phase transitions. This process regulates the interatomic force and changes the potential energy pattern, as shown in Fig. S3b. As the concentration of Te increases, the PESs flatten out and decrease further, so that the atoms can move out of the original H phase. The above results indicate that the phase transition of monolayer WSe_{2-x}Te_x alloys with high Te compositions is quite possible.

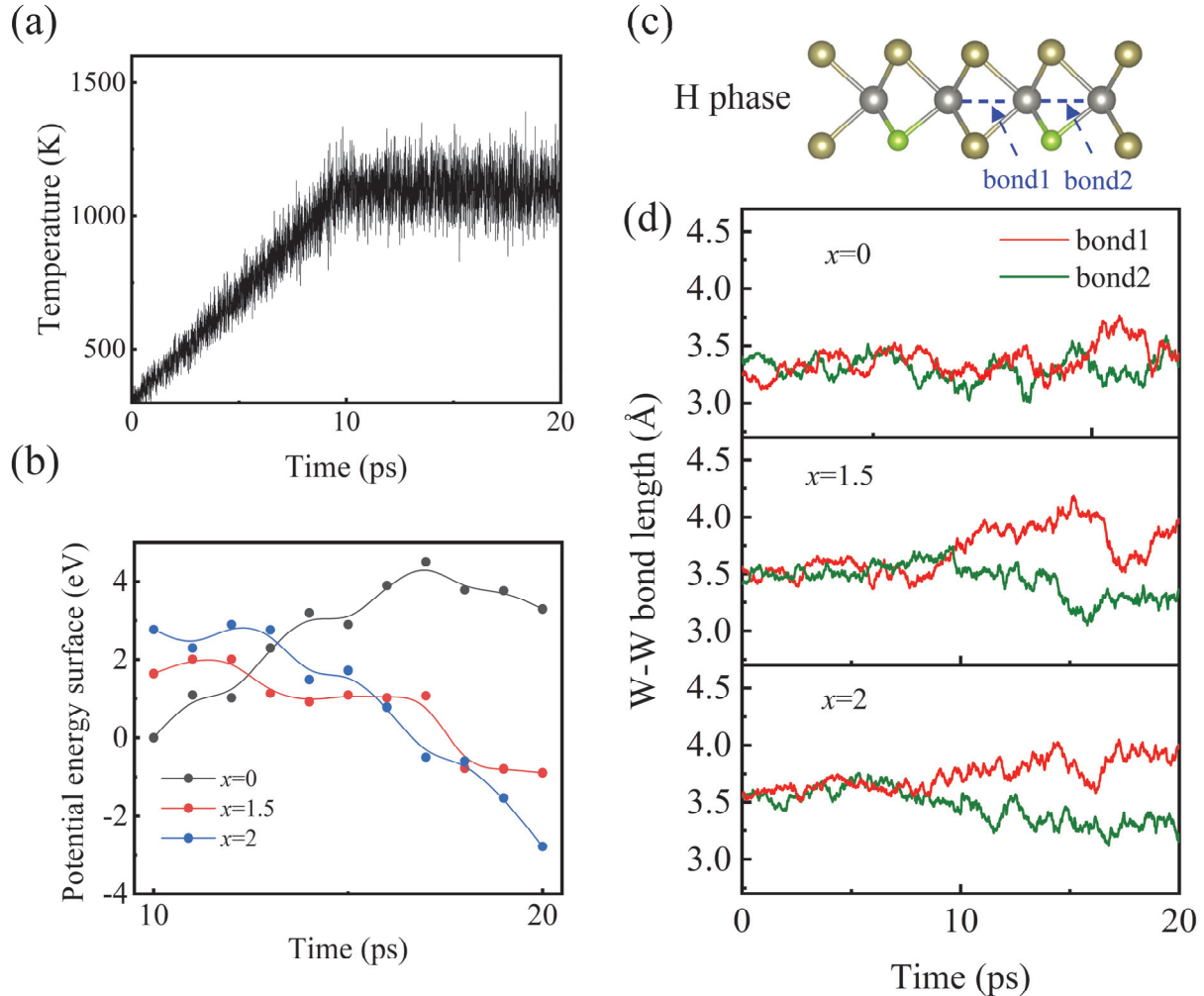


Fig. S3. (a) Temperature curves of AIMD simulations heated from 300 K to 1100 K for H-WSe_{2-x}Te_x monolayers at $x=0$, $x=1.5$ and $x=2$. (b) Curves of the potential energy surfaces (PESs) of WSe_{2-x}Te_x monolayers at $x=0$, $x=1.5$ and $x=2$ under a continuous hot bath at 1100 K. (c) The H phase of WSe_{2-x}Te_x monolayers, bond1 and bond2 represent the evolution of long and short bonds that occur when heated to 1100 K. (d) Dynamic evolution of partial long and short bonds in H-WSe_{2-x}Te_x monolayers heated from 300 K to 1100 K at $x=0$, $x=1.5$, and $x=2$.

Supplementary Note 4

Band structures of H and T' phases of WSe_{2-x}Te_x monolayers:

Fig. S4 shows the electron band structures of the H phases and T' phases of WSe_{2-x}Te_x monolayers. We carry out the generalized gradient approximation of Perdew-Burke-Ernzerhof (GGA-PBE) functional and the screened exchange hybrid Heyd-Scuseria-Ernzerhof (HSE06) functional for the band structure calculations of the WSe_{2-x}Te_x monolayers. When $x=0$, the experimental result show that the band gap of monolayer WSe₂ with H phase as the most stable phase is 1.60 eV, [1] while the band gap values obtained by PBE and HSE06 methods are 1.54 eV and 2.01 eV, respectively. Although the inherent defects of delocalization error and derivative discontinuity, the band gap calculated by PBE method is inevitably underestimated, but within the error range our calculations describe the experimental results well. The H-WSe_{2-x}Te_x monolayers are all semiconductors, and their VBM and CBM are located between the Γ and X points. With the increase of Te concentration, the energy levels of VBM and CBM move upward and the band gap decreases. Similarly, the Fermi levels of T'-WSe_{2-x}Te_x monolayers shift upward with increasing Te concentration. When $x=0.5$ and 1, the T'-WSe_{2-x}Te_x monolayers open up a narrow band gap. The positions of the CBM and VBM levels of the semiconductor phases and the Fermi levels of the semi-metallic phases are closely related to the priority of electron or hole injection. Compared with the HSE06 method, the calculation of PBE method underestimates the band gap, but does not affect the priority of hole or electron doping to occupy the energy level. In addition, considering the time consuming and huge computing resources of HSE06 calculation, we use PBE method for subsequent calculations.

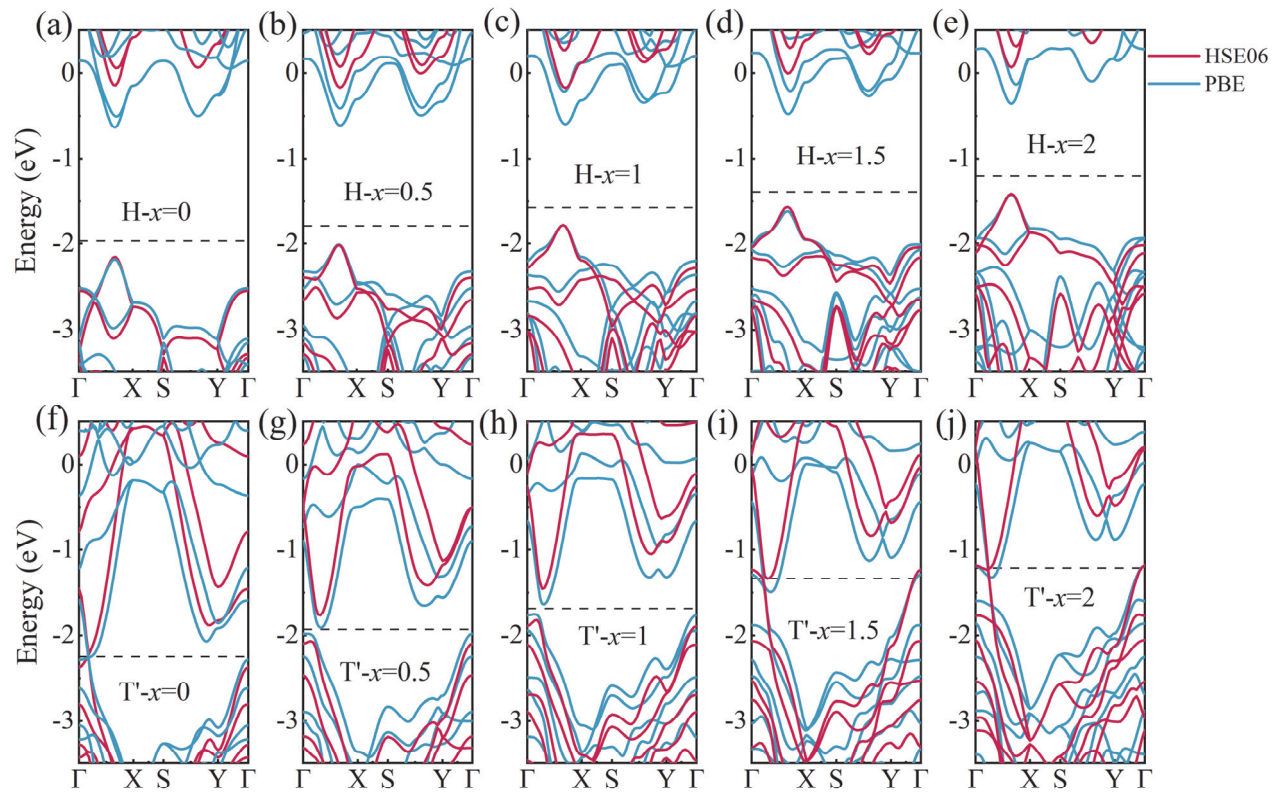


Fig. S4. The band structures of the $\text{WSe}_{2-x}\text{Te}_x$ monolayers in (a-e) H phases and (f-j) T' phases, the red and blue solid lines represent HSE06 and PBE methods, respectively.

Supplementary Note 5

Charge injection and tensile strain regulate the phase transitions for $\text{MoSe}_{2-x}\text{Te}_x$ and $\text{WSe}_{2-x}\text{S}_x$ monolayers:

In order to confirm the feasibility of charge injection and tensile strain for regulating the phase transition for other TMD alloys, we further extend our analysis to $\text{MoSe}_{2-x}\text{Te}_x$ and $\text{WSe}_{2-x}\text{S}_x$ monolayers, as shown in Fig. S5. We select the rectangular unit cell composed of two formula units as research object, and consider the cases of $x=0.5$ and $x=1.5$. After optimized relaxation, the stable geometric structures are shown in Fig. S5a, b. For the neutral case, the H phases of $\text{MoSe}_{2-x}\text{Te}_x$ and $\text{WSe}_{2-x}\text{S}_x$ monolayers are more stable than T phases, as shown in Fig. S5c, d. The energy difference between the two phases decreases with the injection of electrons. When the injected electron concentration exceeds a certain critical value, the T' phase begins to dominate, which is consistent with the $\text{WSe}_{2-x}\text{Te}_x$ monolayers with H phase as the stable phase.

Furthermore, the effect of 4% biaxial tensile strain on the energy barrier of phase transition is considered. As shown in Fig. S5e, f, it is obvious that the biaxial tensile strain can effectively reduce the barrier height of the H to T' phase transition. For $x=0.5$ and $x=1.5$ of $\text{WSe}_{2-x}\text{S}_x$ monolayers, the positive barriers from H to T' phase are 1.30 eV and 1.42 eV, respectively. Under 4% tensile strain, the energy barrier decreases to 1.04 eV and 1.16 eV. Therefore, our results have a certain reference value for accelerating phase transition by reducing the phase transition barrier of monolayer transition metal dichalcogenide alloys by tensile strain.

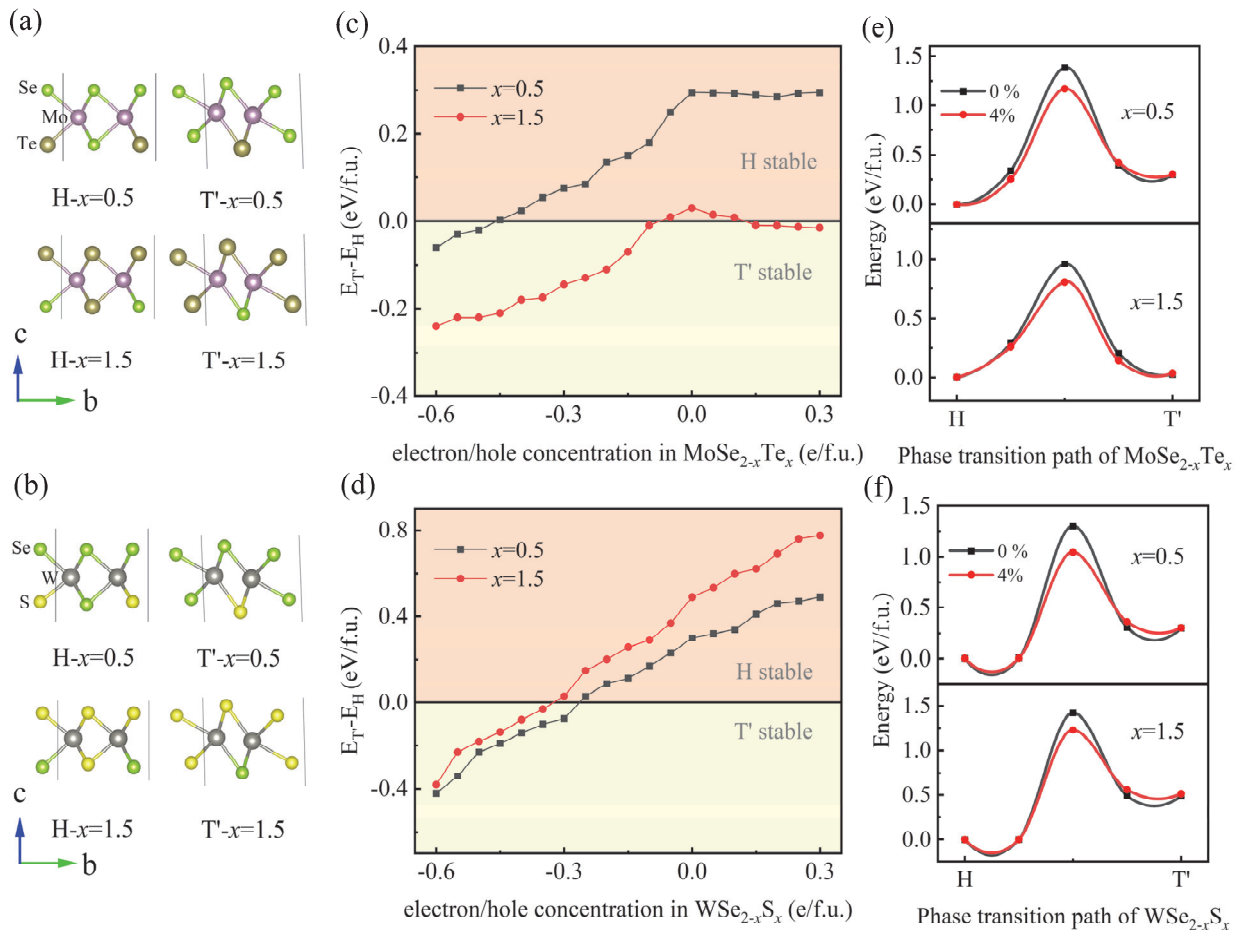


Fig. S5. Atomic structures of (a) $\text{MoSe}_{2-x}\text{Te}_x$ and (b) $\text{WSe}_{2-x}\text{S}_x$ monolayers at $x=0.5$ and $x=1.5$ in H and T' phases. Energy difference between the H- and T'-phases for (c) $\text{MoSe}_{2-x}\text{Te}_x$ and (d) $\text{WSe}_{2-x}\text{S}_x$ monolayers as the function of doping electron and hole concentration. The free energy curves along the transition path from H to T' phases of (e) $\text{MoSe}_{2-x}\text{Te}_x$ and (f) $\text{WSe}_{2-x}\text{S}_x$ monolayers under 0% and 4% tensile strain.

References

- [1] J. K. Huang, J. Pu, C. L. Hsu, M. H. Chiu, Z. Y. Juang, Y. H. Chang, W. H. Chang, Y. Iwasa, T. Takenobu and L. J. Li, *ACS Nano*, 2014, **8**, 923.